Reconstruction of Delayed Neutron Precursor Groups from Data

Luke Seifert,[*,a] Benjamin Betzler,[a] William Wieselquist,[b] Matthew Jessee,[b]
Madicken Munk,[a,c] and Kathryn Huff[a]

[a] *Advanced Reactors and Fuel Cycles Group, University of Illinois at Urbana-Champaign 104 S Wright St, Urbana, IL 61801*

[b] *Nuclear Energy and Fuel Cycle Division, Oak Ridge National Laboratory, Oak Ridge, TN 5200, 1 Bethel Valley Rd, Oak Ridge, TN 37830*

[c] *School of Nuclear Science and Engineering, Oregon State University, Corvallis, OR 211 Merryfield Hall, Corvallis, OR 97331*

[*]Email: seifert5@illinois.edu

Number of pages: 29
Number of tables: 6
Number of figures: 12

Abstract

Delayed neutron precursor (DNP) group data are important for modeling reactor dynamics. Although the data for individual DNPs has been developed over time, the DNP group data present in the Evaluated Nuclear Data Files (ENDF) has not been updated in the past 20 years. This work uses SCALE to recreate the Godiva experiment that was used to generate the original DNP group structure for fast fission of ^{235}U. However, each DNP is modeled using up-to-date data, and the results are then converted into a newly updated group structure. This conversion uses an iterative linear least squares solver to minimize chi-squared. This work also allows for energy spectrum generation and uncertainty tracking. The method used in this paper for fast ^{235}U fission DNP group structure updating can be applied to different energies and fissile nuclides. This work allows for improved uncertainty tracking in reactor kinetics and dynamics simulations, demonstrated through point reactor kinetics simulations.

Keywords — Delayed Neutron Precursors, ORIGEN, SCALE, ENDF, Precursor Group Parameters

I. INTRODUCTION

Delayed neutron precursors (DNPs) make reactor control possible. This is due to the time delay which occurs before a delayed neutron is emitted. DNPs are fission products that are beta-emitting and have sufficient energy to concurrently emit a neutron. Thus, the time delay is based on the half-life of the beta emission. Additionally, some isotopes have sufficient energy to emit multiple neutrons, each of which has different probabilities of occurring.

For many reactor applications, it is practical to divide the DNPs into six to eight groups per fissile isotope instead of modeling each DNP individually. Each of these groups has both a half-life and a yield, or abundance. The half-life of the group is based on the half-lives of the constituent DNPs in that group, while the abundance is based on the amount of DNPs in that group and the average number of neutrons they emit. The differences in group half-lives and abundances are caused by the fission yield differences. These yield differences affect how the DNPs are generated, thus affecting the overall group structure.

The International Atomic Energy Agency (IAEA) maintains a database of DNP data, which has updated data as recent as 2020 and was last updated in 2022 [1]. Although these more recent IAEA data exist, the DNP group data used in the Evaluated Nuclear Data File (ENDF)/B-VIII.0 library have not been updated since ENDF/B-VI.8 [2], approximately 20 years ago [3]. Additionally, the spectral data have not been updated in ∼30 years [4, 5]. This work reconstructs the DNP groups using recent data to evaluate whether the group yield and decay parameters must be altered.

II. METHODS

DNP group data have historically been generated either experimentally or computationally by counting the delayed neutrons after irradiation [6, 7, 5, 8, 9]. Specifically, either a macroscopic or microscopic approach is used [3]. For the macroscopic approach, a fissile sample is irradiated, and the delayed neutron counts are collected. For the microscopic approach, data on individual DNPs is used to simulate a delayed neutron count curve.

Following the generation of delayed neutron counts over time, both approaches then use the same methodologies to generate group fits. In this work, the primary difference in the generated DNP group parameters comes from the data used for the individual DNPs. This work proposes

a new method for generation of DNP group spectral fits. This work also shows how the group fit results from different data compare when used in a point kinetics model. The uncertainties are tracked throughout, as the more recent individual DNP data have uncertainties which can be propagated.

The tools used in this work are in-house Python scripts and SCALE 6.3, within which TRITON and ORIGEN were used for most of the analysis. TRITON is a reactor physics and depletion sequence, and ORIGEN is a depletion and decay solver [10]. Specifically, the "T6-DEPL" TRITON sequence was used that enables TRITON to run with KENO-VI as neutron transport. POLARIS, which handles light water reactor lattice physics, was used for comparing the different DNP group fits after the results were generated.

The primary model of interest in this work is Godiva, a uniform sphere of ^{235}U with a diameter of $6\frac{3}{4}$ inches and density of 19 g/cm^3 [11]. An additional model considered is a generic Westinghouse 17×17 PWR, though the Godiva model is given more attention in this work. The TRITON input deck generated a Godiva geometry and imparted a $0.25ms$ pulse irradiation with roughly 10^{16} fission events. The Godiva sphere does not deplete, but rather a 3 gram sample within Godiva is irradiated, the same as in the Keepin, Wimett, and Zeigler experiment [6]. The irradiation was then followed by a $330s$ decay of the sample using logarithmically spaced time nodes to capture the short-lived DNPs' response in ORIGEN. This method replicated the one used by Keepin, Wimett, and Zeigler so that the results could be directly compared [6]. In the Keepin, Wimett, and Zeigler experiment, the data of interest used for analysis is the delayed neutron count over time.

Using data from the Godiva simulation and recently published experimental data, the delayed neutron count can be constructed. Equation (1) shows how the data comes together to form the delayed neutron count. This equation sums over all DNPs (the number of which can vary based on the dataset), and calculates the time dependent delayed neutron count from each. This contribution from each DNP is then multiplied by the efficiency of the neutron detector, ϵ. By adjusting the detector efficiency term in the equation the delayed neutron count profile is set to align with the results from Keepin, Wimett, and Zeigler [6]. An efficiency term of 3.75×10^{-8} allowed the delayed neutron count rate from the simulation to closely align with the Keepin, Wimett, and Zeigler count rate. Adjusting the efficiency term changes the delayed neutron count rate scaling, but does not

affect the generated group fits themselves.

$$n_d(t) = \epsilon \sum_{i=1}^{I} P_{n_i} \lambda_i N_i(t). \tag{1}$$

In this equation, I represents the total number of DNPs. The concentrations of each DNP, $N_i(t)$, can be retrieved from the ORIGEN binary concentration file. These can then be combined with the emission probabilities, $P_{n,i}$, and decay constants, λ_i, for DNP i from the IAEA database to generate the neutron emission rate as a function of time. This can then be multiplied by the detector efficiency term, ϵ, to generate the delayed neutron count.

The delayed neutron count rate, $n_d(t)$ is calculated in two different ways. The first is using ORIGEN concentrations and IAEA emission probabilities and decay constants. The second is by reading $n_d(t)$ directly from the ORIGEN output, where ORIGEN uses a modified ENDF/B-VII.0 dataset for emission probabilities and decay constants. More specifically, the ORIGEN output uses SCALE 6.2.4 neutron emission, which uses an embedded version of SOURCES4C, combined with a modified ENDF/B-VII.0 dataset [12]. This approach is referred to as *Pure ORIGEN*, as it uses data taken purely from ORIGEN. The other approach which uses ORIGEN concentrations and IAEA data for emission probabilities and decay constants is referred to as *IAEA–ORIGEN*. For DNP data which is in ORIGEN but not the IAEA database, the IAEA-ORIGEN approach obtains data from the Evaluated Nuclear Structure Data File (ENSDF) and ENDF/B-VIII.1 to fill in gaps between the datasets [13, 2].

II.A. Group Fits

Evaluation of the group fits requires generation of the group yield, a_i, and group decay constant, λ_i, for each group. To generate these parameters, this work uses an iterative least squares approach. For a pulse irradiation with n groups and m time nodes, Equations (3)–(7) show how the iterative least squares problem is configured, where the λ_i values are determined by iterating through multiple possible values of each decay constant and checking each combination:

The explicitly formatted pulse irradiation least squares problem is given as

$$n_d(t) \approx \epsilon F_s \sum_{i=1}^{n} a_i \lambda_i e^{-\lambda_i t}, \tag{2}$$

which can be rewritten more generally as

$$A\vec{x} \approx \vec{b}. \tag{3}$$

The a_i, also sometimes given as $\nu_{d,i}$, values are the group yield, or group abundance, values. These represent the number of delayed neutrons per fission; when summed, they provide the total delayed neutron yield per fission. The F_s value is the total number of fission events that take place within the sample, and ϵ is the detector efficiency. The efficiency of the neutron detector in this work, ϵ, is set so that the Keepin, Wimett, and Zeigler delayed neutron precursor count results, when using their group yields and decay constants, align with the reported counts [6]. The total number of delayed neutrons is known by integrating the delayed neutron rate curve. The number of fissions and efficiency term are known as well. The unknowns are the decay constants for each group, λ_i, and the group yields, a_i. However, by iteratively using more refined group decay constants, the problem can be formatted as follows:

$$A = \begin{vmatrix} \lambda_1 e^{-\lambda_1 t_0} & \lambda_2 e^{-\lambda_2 t_0} & \dots & \lambda_n e^{-\lambda_n t_0} \\ \lambda_1 e^{-\lambda_1 t_1} & \lambda_2 e^{-\lambda_2 t_1} & \dots & \lambda_n e^{-\lambda_n t_1} \\ \vdots & \vdots & \ddots & \vdots \\ \lambda_1 e^{-\lambda_1 t_m} & \lambda_2 e^{-\lambda_2 t_m} & \dots & \lambda_n e^{-\lambda_n t_m} \end{vmatrix}, \tag{4}$$

$$\vec{x} = \begin{vmatrix} \nu_{d,1} \\ \nu_{d,2} \\ \vdots \\ \nu_{d,n} \end{vmatrix}, \tag{5}$$

$$\vec{b} = \begin{vmatrix} \frac{n_d(t_0)}{\epsilon F_s} \\ \frac{n_d(t_1)}{\epsilon F_s} \\ \vdots \\ \frac{n_d(t_m)}{\epsilon F_s} \end{vmatrix}, \tag{6}$$

where the solution for the group yields with the guessed group decay constants is:

$$\vec{x} \approx (A^T A)^{-1} A^T \vec{b}. \tag{7}$$

An iterative process is used to improve the guess for the group decay constants such that the net delayed neutron emission curve is better modeled after each iteration. The iteration process goes through Equations (3)–(7) for various values of λ_i; then, the coarseness of the decay constant mesh is decreased, becoming finer until a more optimal solution is found based on minimizing the chi-squared measure, as shown in Equation (8). Equations (9) through (12) define the terms used within the chi-squared calculation. Once a new optimal solution is found, the process begins again with the most coarse mesh, where the λ_i values for a given group i are set to exist within a wide range which becomes smaller after each iteration. The convergence criteria used is to stop when an adjustment of λ_i mesh values by some user defined amount in either direction (i.e., 1% higher and lower) no longer improve the fit. This work used 0.5% for the group fits presented.

$$\chi^2 = \sum_{j=1}^{m} \left(\frac{n_{d,j} - \sum_{i=1}^{n} a_i \lambda_i e^{-\lambda_i t_j}}{\sigma_j} \right)^2, \tag{8}$$

$$m = \text{number of time nodes}, \tag{9}$$

$$n = \text{number of precursor groups}, \tag{10}$$

$$n_{d,j} = \text{delayed neutron counts at time } j, \tag{11}$$

$$\sigma_j = \text{uncertainty in delayed neutron counts at time } j. \tag{12}$$

II.B. Spectral Fits

Group fits are used for the yield and decay constants, but there is also a desire to have group spectra, χ_i. This is referred to in this work as generating a spectral fit. In the past, the spectral fits were generated by allowing each isotope to contribute some fraction of its spectrum to its closest groups, sorted by group half-life [14, 15, 5] or based on nuclide half-life [16, 17]. This work refers to such approaches as *fractional fitting least squares*. Alternatively, using an iterative least squares technique allows for a more optimal set of group fits such that isotopes can contribute to more than

two groups. This method also requires no individualized spectral data for the isotopes, yielding no potential error from erroneous spectral data within the fitting method. This method is referred to as *iterative least squares* in this work.

To determine the energy spectrum of neutrons emitted by each precursor group, the delayed neutron emission rate as a function of time and energy, $n_d(E,t)$, can either be collected from the ORIGEN output or generated from the IAEA database using Equation (13):

$$n_d(E,t) = \epsilon \sum_{i=1}^{I} \chi_i(E)\lambda_i N_i(t) P_{n_i}. \tag{13}$$

In this equation, I represents the total number of DNPs. Once the two-dimensional set of values for $n_d(E,t)$ is collected, the group spectra are generated using iterative least squares. This method iterates through each possible energy bin while solving the least squares problem for every time node, thus optimizing every j^{th} energy bin for all times. Equations (14)–(17) show the iterative least squares method used, whereas Equations (18) and (19) show the solutions using ordinary least squares and using the percent regression least squares, respectively [18]:

$$n_d(E,t) \approx \epsilon F_s \sum_{i=1}^{n} \chi_i(E)\lambda_i a_i e^{-\lambda_i t}, \tag{14}$$

$$A = \begin{vmatrix} \lambda_1\nu_{d,1}e^{-\lambda_1 t_0} & \lambda_2\nu_{d,2}e^{-\lambda_2 t_0} & \dots & \lambda_n\nu_{d,n}e^{-\lambda_n t_0} \\ \lambda_1\nu_{d,1}e^{-\lambda_1 t_1} & \lambda_2\nu_{d,2}e^{-\lambda_2 t_1} & \dots & \lambda_n\nu_{d,n}e^{-\lambda_n t_1} \\ \vdots & \vdots & \ddots & \vdots \\ \lambda_1\nu_{d,1}e^{-\lambda_1 t_m} & \lambda_2\nu_{d,2}e^{-\lambda_2 t_m} & \dots & \lambda_n\nu_{d,n}e^{-\lambda_n t_m} \end{vmatrix}, \tag{15}$$

$$\vec{x} = \begin{vmatrix} \chi_1(E_j) \\ \chi_2(E_j) \\ \vdots \\ \chi_n(E_j) \end{vmatrix}, \tag{16}$$

$$\vec{b} = \begin{vmatrix} \frac{n_d(E_j,t_0)}{\epsilon F_s} \\ \frac{n_d(E_j,t_1)}{\epsilon F_s} \\ \vdots \\ \frac{n_d(E_j,t_m)}{\epsilon F_s} \end{vmatrix}, \tag{17}$$

$$\vec{x} \approx (A^T A)^{-1} A^T \vec{b}, \tag{18}$$

$$\vec{x} = (A^T D^2 A)^{-1} A^T D^2 \vec{b}. \tag{19}$$

In the percent regression least squares formulation, D is a diagonal matrix containing the inverse of $\vec{b}$ along the diagonal, as shown in Equation (20).

$$D = \begin{vmatrix} \frac{\epsilon F_s}{n_d(E_j,t_0)} & 0 & \dots & 0 \\ 0 & \frac{\epsilon F_s}{n_d(E_j,t_1)} & \dots & 0 \\ \vdots & \vdots & \ddots & \vdots \\ 0 & 0 & \dots & \frac{\epsilon F_s}{n_d(E_j,t_m)} \end{vmatrix} \tag{20}$$

Equation (19) was incorporated into the non-negative least squares method in the outer loop, whereas the residual in the outer loop was adjusted to solve the residual equation shown in Equation (21) [19]:

$$argmin_x \left|\left| \frac{Ax - b}{b} \right|\right|_2. \tag{21}$$

This approach is computatoinally costly, can calculate a negative group spectrum probability, and can be inaccurate at long times. Although the computational cost issue will remain, the other issues can be solved by implementing a combination of non-negative least squares and least squares percentage regression techniques [19, 18]. However, a more optimal solution is generated by instead implementing the least squares percentage regression and then setting any negative emission probability bin values to 0.

II.C. Point Reactor Kinetics

Using the point reactor kinetics equations enables an understanding of how the group fits will affect the system on a more macroscopic scale. Equation (22) provides the initial conditions used, whereas Equations (23) and (24) are the general forms of the neutron density and precursor concentrations equations, respectively:

$$\begin{aligned} n_0 &= 1 \\ c_{i_0} &= \beta_i n_0 \left(\lambda_i \Lambda\right)^{-1}, \end{aligned} \tag{22}$$

$$\frac{dn}{dt} = \frac{\rho - \beta}{\Lambda} n(t) + \sum_{i=1}^{6} \lambda_i C_i(t), \tag{23}$$

$$\frac{dC_i}{dt} = \frac{\beta_i}{\Lambda} n(t) - \lambda_i C_i(t). \tag{24}$$

The Λ term is the neutron generation time, ρ is the reactivity, and the β_i values are calculated using the group yields and average neutron emission per fission event, as shown in Equation (40):

$$\beta_i = \frac{a_i}{\bar{\nu}}. \tag{25}$$

In this work, the equations were solved iteratively, and each subsequent term was calculated using the forward Euler method, shown in Equations (26) and (27):

$$n^{(m)} = n^{(m-1)} + \frac{dn^{(m-1)}}{dt} \Delta t, \tag{26}$$

$$C_{i^{(m)}} = C_{i^{(m-1)}} + \frac{dC_{i^{(m-1)}}}{dt} \Delta t. \tag{27}$$

The forward Euler method is not an optimal approach to generating results for the point reactor kinetics equations; however, generating and providing results that demonstrate the differences yielded from each data set is simple using this approach.

II.D. Uncertainties

An important consideration for the group fit methods are the uncertainties in the data used. The group fit uncertainty has contributions from decay constants, delayed neutron emission counts, and fissions [20].

The uncertainty in the delayed neutron emission counts from ORIGEN can be determined based on Equation (13) by using Equations (28)–(31). This uncertainty is then used in Equations (32)–(35) to calculate the uncertainty for the entire right-hand side of the least squares problem given in Equation (3).

The uncertainty in the emission probabilities, ΔP_{n_i}, comes from the IAEA data; the uncertainty in concentration, ΔN_{0_i}, comes from Sampler in SCALE [10], a tool that statistically samples the input data for general uncertainty analysis; and the uncertainty in the decay constants, $\Delta\lambda_i$, comes from the IAEA data for the ORIGEN delayed neutron counts and is based on the mesh for the group fit. Sampler is used with 500 samples, with perturbations in each non-metastable nuclide of cross sections, yields, and decay constants.

Partial derivatives of each term in Equation (13) yield Equations (28)–(30). These partial derivatives are then used in the uncertainty calculation in the delayed neutron count from each individual delayed neutron precursor as shown in Equation (31).

$$\frac{\partial n_d(t)}{\partial P_{n_i}} = \lambda_i N_{0_i} e^{-\lambda_i t}, \tag{28}$$

$$\frac{\partial n_d(t)}{\partial \lambda_i} = P_{n_i} N_{0_i} (1 - \lambda_i t) e^{-\lambda_i t}, \tag{29}$$

$$\frac{\partial n_d(t)}{\partial N_{0_i}} = P_{n_i} \lambda_i e^{-\lambda_i t}, \tag{30}$$

$$\begin{aligned} \Delta n_d^2(t) = \epsilon \sum_{i=1}^{n} \left(\frac{\partial n_d(t)}{\partial P_{n_i}} \Delta P_{n_i} \right)^2 + \left(\frac{\partial n_d(t)}{\partial \lambda_i} \Delta \lambda_i \right)^2 \\ + \left(\frac{\partial n_d(t)}{\partial N_{0_i}} \Delta N_{0_i} \right)^2. \end{aligned} \tag{31}$$

Equation (32) is the right-hand side vector at a point in time m used when fitting the group constants. Partial derivatives are taken, shown in Equations (33) and (34). These partial derivatives are then used to generate the uncertainty at that time, shown in Equation (35).

$$\vec{b}_m = \frac{n_d(t_m)}{\epsilon F_s}. \tag{32}$$

$$\frac{\partial \vec{b}_m}{\partial n_d(t_m)} = \frac{1}{\epsilon F_s}, \tag{33}$$

$$\frac{\partial \vec{b}_m}{\partial F_s} = -\frac{n_d(t_m)}{\epsilon F_s^2}, \tag{34}$$

$$\Delta\vec{b}_m = \frac{1}{\epsilon}\sqrt{\left(\frac{\partial \vec{b}_m}{\partial n_d(t_m)}\Delta n_d(t_m)\right)^2 + \left(\frac{\partial \vec{b}_m}{\partial F_s}\Delta F_s\right)^2}. \tag{35}$$

The uncertainty in the delayed neutron emission counts from the group fit can be found using Equations (2) and the partial derivatives in Equations (36)–(37), yielding the result in Equation (38).

$$\frac{\partial n_d}{\partial a_i} = \lambda_i e^{-\lambda_i t}, \tag{36}$$

$$\frac{\partial n_d}{\partial \lambda_i} = a_i(1-\lambda_i t)e^{-\lambda_i t}, \tag{37}$$

$$\Delta n_d(t) = \epsilon F_s \sqrt{\sum_{i=1}^{n}\left(\frac{\partial n_d}{\partial a_i}\Delta a_i\right)^2 + \left(\frac{\partial n_d}{\partial \lambda_i}\Delta\lambda_i\right)^2}. \tag{38}$$

The uncertainty in the group yield values, Δa_i, was calculated stochastically. The least squares problem used to solve for a_i was iterated upon with random variations within uncertainties for the various terms until the point at which a normal distribution formed and the standard deviation could be directly extracted. An example of this approach is shown Figure 1, in which the sixth group yield is $(4.3 \pm 0.4) \times 10^{-4}$ delayed neutrons per fission.

Following the group fit are the point reactor kinetics uncertainties that use forward Euler.

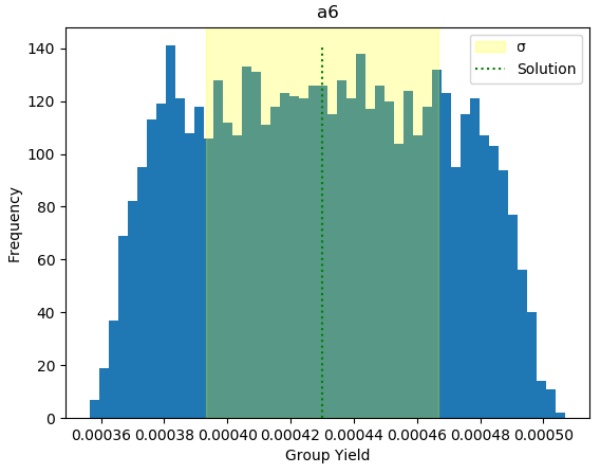

Fig. 1. 5,000 stochastic uncertainty simulations of the Keepin, Wimett, and Zeigler sixth precursor group yield using a 0.5% half-life step size.

The decay constant uncertainty comes from the group fits; the initial uncertainties in both the number of neutrons at the current time, $\Delta n^{(m)}$, and the number of precursors in the i^{th} group, $\Delta C_i^{(m)}$, are zero; and the group and total delayed neutron fraction uncertainties, $\Delta\beta_i$ and $\Delta\beta$, respectively, are given in Equations (39) and (40):

$$\Delta\beta_i = \sqrt{\left(\frac{1}{\bar{\nu}}\Delta a_i\right)^2 + \left(\frac{a_i}{\bar{\nu}^2}\Delta\bar{\nu}\right)^2}, \tag{39}$$

$$\Delta\beta = \sqrt{\left(\sum_{i=1}^{n}\Delta\beta_i^2\right)}. \tag{40}$$

The uncertainty in $n^{(m)}$ from Equation (26), rewritten explicitly in Equation (41), is given in Equation (47), with the components given in Equations (42)–(46). In these equations, Δt is the time step used in forward Euler:

$$\begin{aligned} n^{(m)} &= n^{(m-1)} + \frac{\rho-\beta}{\Lambda}n^{(m-1)}\Delta t \\ &+ \sum_{i=1}^{n}\left(\lambda_i C_i^{(m-1)}\Delta t + \frac{\beta_i}{\Lambda}n^{(m-1)}\lambda_i\Delta t^2 - \lambda_i^2 C_i^{(m-1)}\Delta t^2\right), \end{aligned} \tag{41}$$

$$\frac{\partial n^{(m)}}{\partial n^{(m-1)}} = 1 + \frac{\rho - \beta}{\Lambda}\Delta t + \sum_{i=1}^{n} \frac{\beta_i}{\Lambda}\lambda_i \Delta t^2, \tag{42}$$

$$\frac{\partial n^{(m)}}{\partial \lambda_i} = C_i^{(m-1)}\Delta t + \frac{\beta_i}{\Lambda} n^{(m-1)}\Delta t^2 - 2\lambda_i C_i^{(m-1)}\Delta t^2, \tag{43}$$

$$\frac{\partial n^{(m)}}{\partial \beta} = \frac{-n^{(m-1)}\Delta t}{\Lambda}, \tag{44}$$

$$\frac{\partial n^{(m)}}{\partial \beta_i} = \frac{n^{(m-1)}\lambda_i \Delta t^2}{\Lambda}, \tag{45}$$

$$\frac{\partial n^{(m)}}{\partial C_i^{(m-1)}} = \lambda_i \Delta t - \lambda_i^2 \Delta t^2, \tag{46}$$

$$\begin{aligned}\left(\Delta n^{(m)}\right)^2 = &\sum_{i=1}^{n} \left(\frac{\partial n(t)}{\partial n^{(m-1)}}\Delta n^{(m-1)}\right)^2 + \left(\frac{\partial n(t)}{\partial \lambda_i}\Delta \lambda_i\right)^2 \\ &+ \left(\frac{\partial n(t)}{\partial \beta}\Delta \beta\right)^2 + \left(\frac{\partial n(t)}{\partial \beta_i}\Delta \beta_i\right)^2 \\ &+ \left(\frac{\partial n(t)}{\partial C_i^{(m-1)}}\Delta C_i^{(m-1)}\right)^2.\end{aligned} \tag{47}$$

The uncertainty in C_i from (27), rewritten explicitly in Equation (48), is given by Equation (53), incorporating the components given by Equations (49)–(52):

$$C_i^{(m)} = C_i^{(m-1)} + \frac{\beta_i}{\Lambda} n^{(m-1)}\Delta t - \lambda_i \Delta t C_i^{(m-1)}, \tag{48}$$

$$\frac{\partial C_i^{(m)}(t)}{\partial C_i^{(m-1)}} = 1 - \lambda_i \Delta t, \tag{49}$$

$$\frac{\partial C_i^{(m)}}{\partial \beta_i} = \frac{n^{(m-1)}\Delta t}{\Lambda}, \tag{50}$$

$$\frac{\partial C_i^{(m)}}{\partial n^{(m-1)}} = \frac{\beta_i \Delta t}{\Lambda}, \tag{51}$$

$$\frac{\partial C_i^{(m)}}{\partial \lambda_i} = -C_i^{(m-1)} \Delta t, \tag{52}$$

$$\begin{aligned}\left(\Delta C_i^{(m)}\right)^2 = \sum_{i=1}^{n} &\left(\frac{\partial C_i^{(m)}}{\partial n^{(m-1)}} \Delta n^{(m-1)}\right)^2 + \left(\frac{\partial C_i^{(m)}}{\partial \lambda_i} \Delta \lambda_i\right)^2 \\ &+ \left(\frac{\partial C_i^{(m)}}{\partial \beta_i} \Delta \beta_i\right)^2 + \left(\frac{\partial C_i^{(m)}}{\partial C_i^{(m-1)}} \Delta C_i^{(m-1)}\right)^2.\end{aligned} \tag{53}$$

Finally, the uncertainty of group spectra constructed using the iterative linear least squares procedure is shown in Equation (54). This uncertainty is fairly straightforward to calculate because the delayed neutron count term, $n_d(t)$, comes from the six group fit for which the uncertainty is given in Equation (38). The uncertainty for the energy-dependent neutron emission counts is shown in Equation (55), where the uncertainty in the spectra, $\Delta\chi_i(E)$, is calculated stochastically, in the same manner as the group yield uncertainties:

$$n_d(E,t) = n_d(t) \sum_i \chi_i(E), \tag{54}$$

$$\Delta n_d^2(E,t) = \left(\Delta n_d(t) \sum_i \chi_i(E)\right)^2 + \left(n_d(t)\right)^2 \sum_i \left(\Delta\chi_i(E)\right)^2. \tag{55}$$

III. RESULTS AND ANALYSIS

III.A. ORIGEN Data Compared with IAEA Data

Because the group fits are fit to the delayed neutron count data, it is important to understand how the data compare. The two different datasets compared are the IAEA database and the end7dec default decay ORIGEN library—referred to as *Pure ORIGEN*, *Pure*, or simply *ORIGEN*—which uses modified ENDF/B-VII.0 data and an embedded version of SOURCES4C. For analysis of delayed neutron emission counts, the three components that can change because of data are the

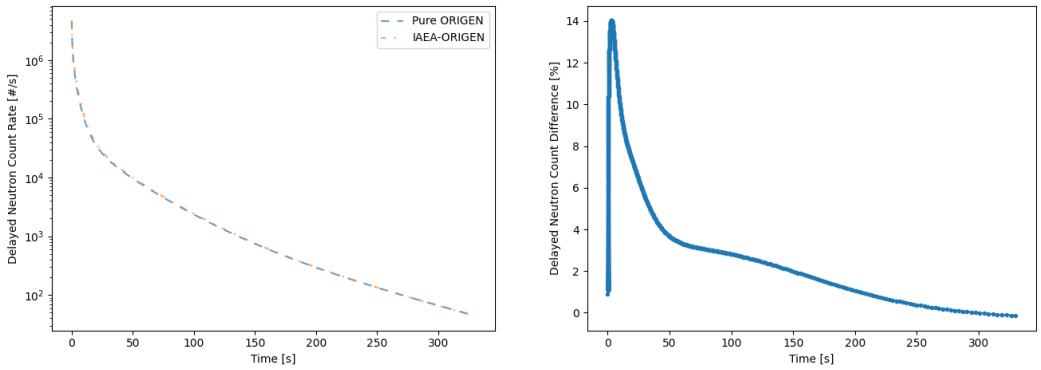

(a) Pure ORIGEN and IAEA ORIGEN count rate over time

(b) Pure ORIGEN and IAEA ORIGEN count rate difference over time

Fig. 2. Comparison of delayed neutron count rate for Pure ORIGEN and IAEA ORIGEN data after fast-pulse irradiation of ^{235}U.

time-dependent compositions, the decay constants, and the emission probabilities, all of which can be seen in Equation (1).

The composition as a function of time depends on the incident fission neutron energy, the fission yield, the decay constant of the target isotope, and that same data for any isotopes that decay into the target isotope. In this work, the ORIGEN- and IAEA-based data comparisons use the compositions generated by KENO-VI and decayed in ORIGEN.

The decay constants, λ, and emission probabilities (or branching fractions), P_n, can be tested by comparing the results of the Pure ORIGEN dataset simulated in ORIGEN with the IAEA dataset in ORIGEN. Specifically, we can adjust the data such that only decay constants, only emission probabilities, or both are swapped from the Pure ORIGEN dataset values to the IAEA dataset values.

Figure 2 shows the net counts for the Pure ORIGEN and for the IAEA–ORIGEN data sets in which the percent difference appears to be close. The percent difference between the count rates was small at first, peaked at a 14% difference, and then dropped again. From the shape of the percent difference, it appears that short-lived isotopes decay away and reduce the difference.

Figures 3–5 provide more information on the short-lived and longer-lived isotopes that caused the discrepancy between the different sets of data by showing the delayed neutron count rates. Figure 3 shows that the peak decay constant difference causes around 1.2 million counts per second, while the difference drops rapidly during later times. The emission probabilities have a smaller

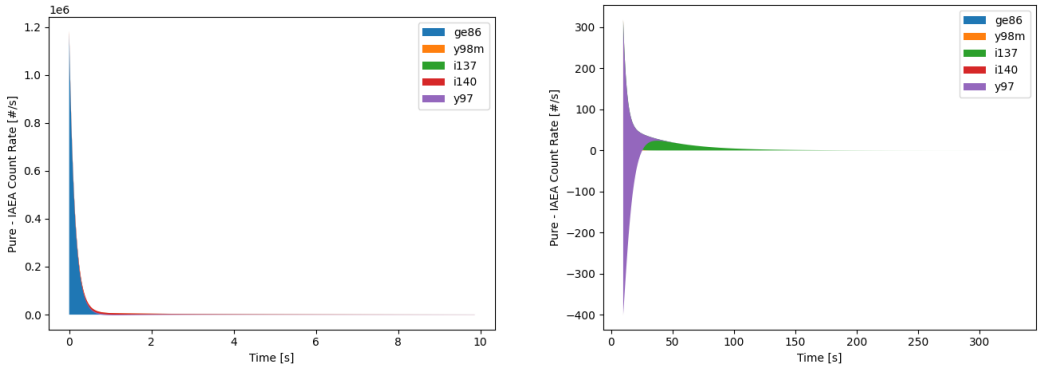

(a) Short time scale (b) Long time scale

Fig. 3. Decay constant–based difference between count rates with IAEA decay constants for ^{235}U fast-pulse irradiation over different time frames.

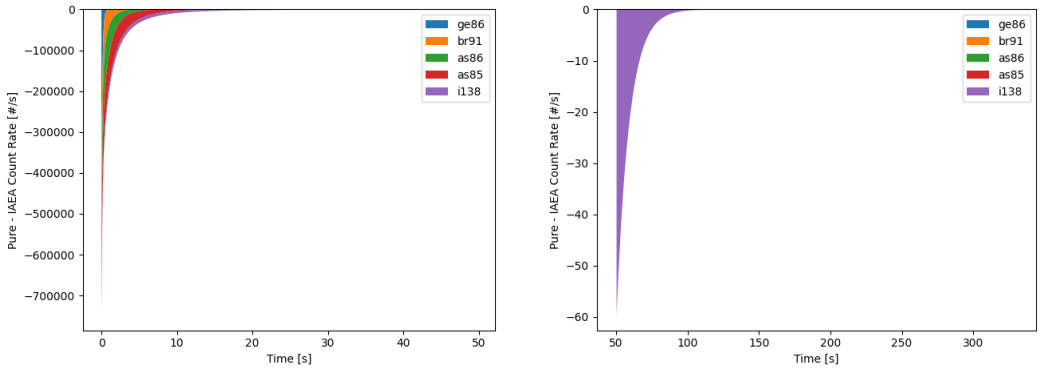

(a) Short time scale (b) Long time scale

Fig. 4. Emission probability (i.e., branching fraction)–based difference between count rates with IAEA decay constants for ^{235}U fast-pulse irradiation over different time frames.

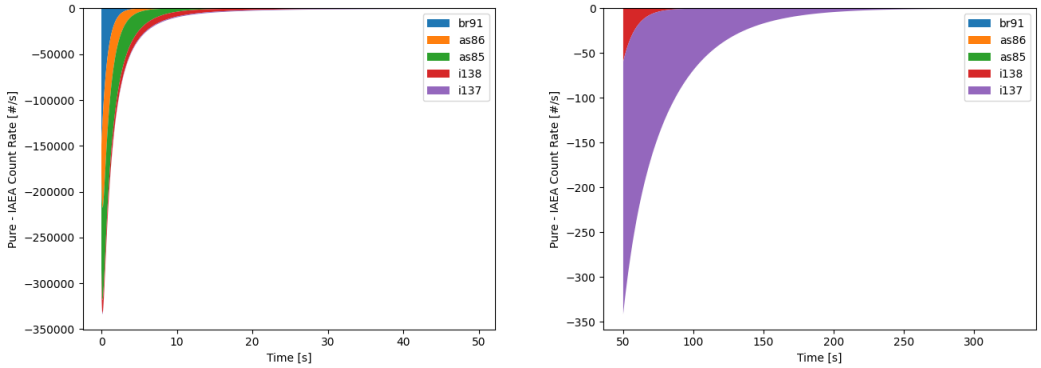

(a) Short time scale (b) Long time scale

Fig. 5. Combined decay constant and emission probability–based difference between count rates with IAEA decay constants for ^{235}U fast-pulse irradiation over different time frames.

TABLE I
Difference in data for isotopes with the largest difference in counts.

Isotope	λ_{IAEA}	λ_{ORIGEN}	$\Delta\lambda$	P_{IAEA}	P_{ORIGEN}	ΔP
^{91}Br	1.27	1.28	0.01	0.304	0.109	0.195
^{85}As	0.343	0.343	0.00	0.625	0.22	0.405
^{86}As	0.734	0.733	0.001	0.345	0.105	0.240
^{137}I	0.028	0.028	0.00	0.076	0.072	0.004
^{138}I	0.111	0.111	0.00	0.053	0.026	0.027
^{86}Ge	3.12	7.30	4.18	0.45	0.22	0.23
^{98m}Y	0.299	0.347	0.048	0.034	0.034	0.00
^{140}I	1.17	0.806	0.364	0.079	0.22	0.141
^{97}Y	0.185	0.185	0.00	5.8E-4	0.003	0.00242

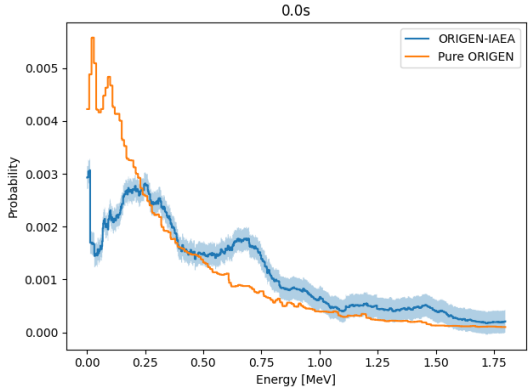

Fig. 6. Normalized difference in emission spectra of Pure ORIGEN and IAEA–ORIGEN for ^{235}U fast-pulse irradiation at 0 s.

maximum effect, but the integral effect is larger; therefore, the combined effects of emission and decay constants are dominated by precursors that are significantly affected by emission probability data differences.

Table I lists the isotopes that have the most significant effect on the decay constant and emission probability data differences. Figures 4 and 5 show the impact these nuclides have on the delayed neutron count rate. Based on Table I, it can be seen that the main difference in the delayed neutron count rates is caused by emission probabilities. This is because the predominant net difference is a result of the emission probability, which is further shown in Table II, where changing the decay data source only slightly affects the total delayed neutron yield while changing the emission probability data source changes the yield by approximately 200 pcm.

Figure 6 shows how the initial spectra of the ORIGEN output vary from the IAEA–ORIGEN spectra. Although these results account for only one time step, the spectral differences become

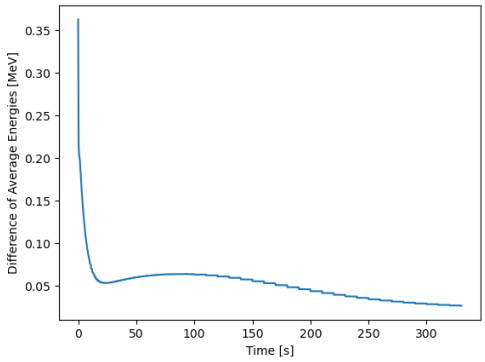

Fig. 7. Difference in average neutron energy of Pure ORIGEN and IAEA–ORIGEN for ^{235}U fast-pulse irradiation over time where Pure ORIGEN is subtracted from IAEA–ORIGEN.

TABLE II
Net yields from various sources of data (partially recreated from [15]).

λ	P_n	Yield
IAEA	IAEA	0.0191
ORIGEN	IAEA	0.0193
IAEA	ORIGEN	0.0172
ORIGEN	ORIGEN	0.0172
Keepin, Wimett, and Zeigler [6]	Keepin, Wimett, and Zeigler [6]	0.0165
Brady and England [15]	Brady and England [15]	0.0206
Tuttle [21]	Tuttle [21]	0.0167
ENDF/B-V [22]	ENDF/B-V [22]	0.0167
England et al. [23]	England et al. [23]	0.0198
England and Rider [24]	England and Rider [24]	0.0206

smaller over time, as shown in Figure 7. This discrepancy at short time steps aligns with the previously discussed results. Additionally, because the main differences occur in the first 2 s, the problematic isotopes can be determined directly. The results shown in Figures 3–5 indicate that those isotopes that differ most significantly within the first 2 s are ^{91}Br, ^{85}As, ^{86}As, ^{137}I, and ^{138}I.

III.B. Six Group Fits

The DNP six groups can be calculated using the generated delayed neutron count rate data and iterative least squares method. An efficiency term of 3.75E-8 was used to align the group fit with the data presented in the Keepin, Wimett, and Zeigler paper [6]. This efficiency term was also used for the other results so that they could all be compared directly.

Table II lists the net yield variance observed between the IAEA data and ORIGEN library

TABLE III
Six group fit half-life parameters given in seconds.

Fit	T_1	T_2	T_3	T_4	T_5	T_6
[15]	52.1	21.2	5.74	2.29	0.816	0.243
[6]	54.5	21.8	6.00	2.23	0.496	0.179
IAEA	49.0	19.2	3.64	1.28	0.320	0.098
Pure	51.3	20.7	6.04	2.19	0.505	0.115

TABLE IV
Six group fit half-life parameters' uncertainties given in seconds.

Fit	ΔT_1	ΔT_2	ΔT_3	ΔT_4	ΔT_5	ΔT_6
[6]	0.94	0.54	0.17	0.06	0.03	0.02
IAEA	0.245	0.096	0.018	0.006	0.002	0.001
Pure	0.256	0.104	0.030	0.011	0.003	0.001

data. Additionally, net yields from other works are shown for fast ^{235}U irradiation.

Emission probability is the principal reason yield varied between the IAEA data and the ORIGEN decay library; a shift in the decay constant data minimally affects the net yield. Additionally, the net yields range from 0.0165 to 0.206 in the literature, which is a fairly large range of values. The current work's values fall within this range.

Tables III and V contain the group fit parameters, which were identified using the iterative least squares approach and the group fit parameters taken from Brady and England and from Keepin, Wimett, and Zeigler [15, 6]. The uncertainties for the group fits are given in Tables IV and VI.

In the group half-life fitting performed by the IAEA, each group exhibited a shorter half-life compared with all other fits. For the group yields, the IAEA fit showed greater weight on the longer-lived groups, which is noticeable when comparing the longest- and shortest-lived group yields. A comparison of the fits is shown in Figure 8; this comparison indicates that the current work's group fits are similar to other methods. The comparison also reveals discrepancies among

TABLE V
Six group fit yield parameters in delayed neutrons per fission multiplied by 100.

Fit	a_1	a_2	a_3	a_4	a_5	a_6
[15]	0.072	0.372	0.355	0.797	0.327	0.137
[6]	0.063	0.351	0.310	0.672	0.211	0.043
IAEA	0.083	0.350	0.670	0.566	0.187	0.054
Pure	0.071	0.308	0.244	0.711	0.300	0.091

TABLE VI
Six group fit yield parameters' uncertainties in delayed neutrons per fission multiplied by 100.

Fit	Δa_1	Δa_2	Δa_3	Δa_4	Δa_5	Δa_6
Keepin	0.005	0.011	0.028	0.023	0.015	0.005
IAEA	0.009	0.009	0.008	0.003	0.003	0.001
Pure	0.014	0.018	0.012	0.007	0.002	0.001

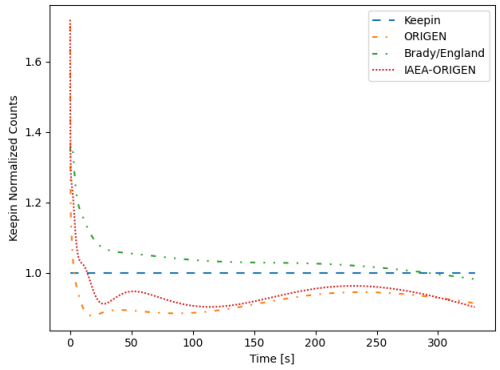

Fig. 8. A comparison of the different fast fission irradiation DNP six group fits of ^{235}U normalized to the Keepin, Wimett, and Zeigler six group fit count rate [6].

the other referenced fits, although all of the fits shown are for the same fissile isotope and fast energy spectrum.

The discrepancies could be the result of differences in energy spectra causing fission, uncertainty in the number of fission events, uncertainty in the experimental data collected by Keepin, Wimett, and Zeigler (which were fitted), or uncertainty in the nuclear data used in the codes in this work and in Brady and England's work.

III.C. Six Group Spectra

Using the six group fits generated, as well as the energy-dependent count rate from ORIGEN and the constructed data from the IAEA database, the spectral profiles associated with each group can be generated, as shown in Equation (14). Figure 9 shows a comparison of the fractional fitting method and the iterative least squares method, labeled as Data Fit, implemented in this work.

Figure 10 further compares the discrepancy between the historical fractional fitting approach and the proposed iterative least squares approach. The iterative least squares provided a much better fit than that of the fractional fitting method. This is shown at 330 s, but it is valid across the other times as well.

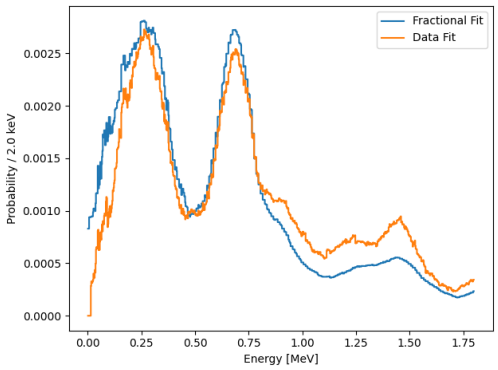

Fig. 9. Comparison of fractional fitting least squares method and iterative least squares method for the sixth precursor group for IAEA-ORIGEN in ^{235}U fast-pulse irradiation.

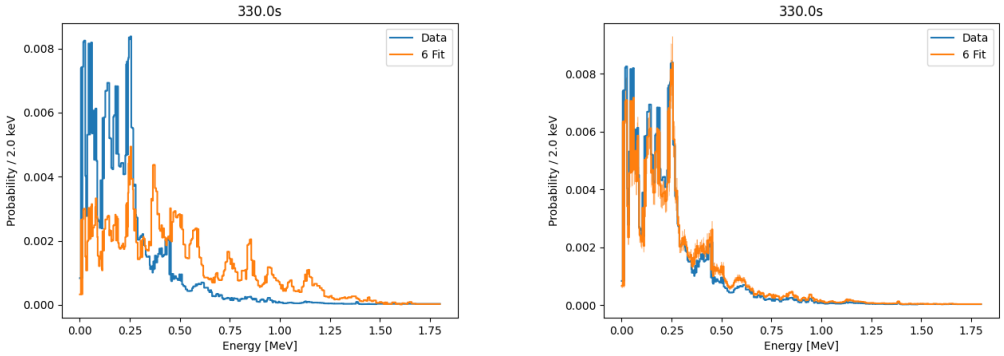

(a) Fractional fitting

(b) Iterative least squares

Fig. 10. Comparison of data with normalized IAEA-ORIGEN six group spectra for ^{235}U pulse irradiation at 330 seconds.

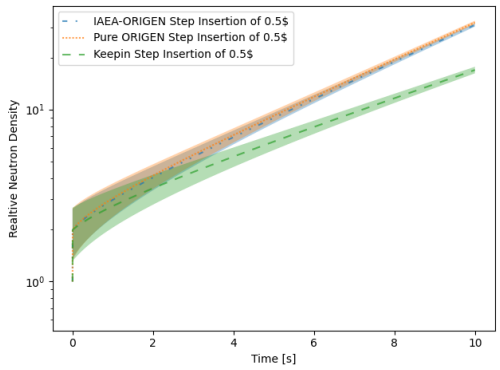

Fig. 11. Point reactor kinetic neutron density response to reactivity step insertion for different six group fits.

III.D. Point Reactor Kinetics Reactivity Insertion

To produce a macroscopic view of the effect of altering the group fit, the response to a reactivity step insertion can be modeled using point reactor kinetics. Figure 11 shows the neutron density response to a reactivity step insertion into a reactor with a neutron generation time of 0.1 μs and average number of total neutrons per fission of 2.6.

Figure 11 shows that the Keepin, Wimett, and Zeigler response was slightly lower than that of the current work [6]. The responses began closely aligned and diverged further apart as the effect of the DNPs becomes more significant. In the later times, the IAEA–ORIGEN neutron density was slightly lower than the Pure ORIGEN neutron density. This is because the group fit of Pure ORIGEN has higher yield values for five and six groups, the yield values of which dominate during the early times. This effect was counteracted slightly by the slightly longer lives of five and six groups that Pure ORIGEN also has, but the net effect was still an increased response compared with that of the IAEA–ORIGEN group fit. Following this logic, the Keepin, Wimett, and Zeigler group fit has small yields for five and six groups while also having fairly long half- lives for each group.

III.E. Westinghouse 17 × 17 Pressurized Water Reactor

Additional macroscopic analysis was conducted using SCALE/Polaris. SCALE/Polaris is a tool used to perform 2D lattice physics that provides six group kinetics parameters as an output. These outputs are importance weighted, nuclide integrated, and assembly homogenized. Because

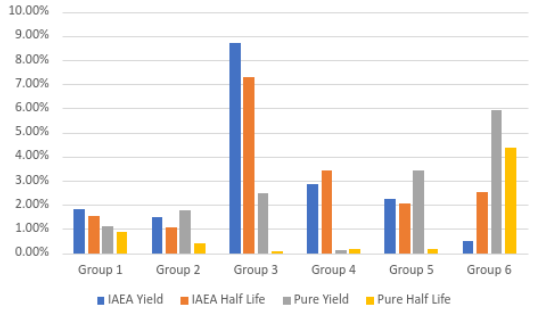

Fig. 12. The absolute percent difference of IAEA and Pure ORIGEN six group fits to the Keepin, Wimett, and Zeigler fits of fast spectrum U^{235} in a Westinghouse 17×17 fuel assembly.

these kinetics parameters are used by other codes to perform transient analyses, it is important to determine the difference using the default kinetic parameters used as an input compared with the six group fits generated in this work.

For this analysis, only the fast-spectrum kinetics parameters were altered for ^{235}U. This adjustmented was performed to provide a conservative estimate for the magnitude of difference, which can be expected because of the heavily thermal spectrum.

The default values used for the kinetic parameter inputs are those from Keepin, Wimett, and Zeigler [6]. The IAEA and Pure ORIGEN six group fits presented in this work were then used. The resulting kinetics parameters outputs for each set of group fits were compared with the absolute percent differences shown in Figure 12.

These absolute percent differences from the Keepin, Wimett, and Zeigler data show that the largest difference in IAEA yield and half-life values was observed in the third precursor group; the greatest difference in those values for Pure ORIGEN was observed in the sixth precursor group. This result corresponds directly to the differences in the six group fits shown in Tables III and V.

IV. CONCLUSIONS AND FUTURE WORK

This work demonstrates generation of DNP group parameters from a simulated irradiation combined with external data. The updated DNP data from the IAEA database differs from previous data; in particular, a few particular nuclides have large differences. The nuclides with the largest data discrepancies include ^{91}Br, ^{85}As, ^{86}As, ^{137}I, ^{138}I, ^{86}Ge, ^{98m}Y, ^{140}I, and ^{97}Y. Discrepancies among the data between SOURCES4C and the ENDF are currently being dealt with by relying more on ENDF and less on SOURCES4C where possible in SCALE. Additionally, corresponding

updates could be made to the group fits by implementing updated data and propagating uncertainty. The group spectra could also be updated with uncertainty propagation and methods for fitting optimal group spectra.

A more thorough analysis of various group fitting methods for yields, abundances, and spectra could include using non-linear least squares or other least squares methods, calculating uncertainty when the decay constant mesh is refined to the furthest extent possible, and determining whether other methods would alter how many groups are needed for a fit within a given margin. Analysis of additional data sources, such as the Joint Evaluated Fission and Fusion library, could similarly identify additional isotopes causing discrepancies.

ACKNOWLEDGMENTS

This manuscript has been authored by UT-Battelle, LLC under contract DE-AC05-00OR22725 with the US Department of Energy (DOE). The US government retains and the publisher, by accepting the article for publication, acknowledges that the US government retains a nonexclusive, paid-up, irrevocable, worldwide license to publish or reproduce the published form of this manuscript, or allow others to do so, for US government purposes. DOE will provide public access to these results of federally sponsored research in accordance with the DOE Public Access Plan (http://energy.gov/downloads/doe-public-access-plan). This material is based upon work supported under an Integrated University Program Graduate Fellowship. The authors are grateful for this generous support. Thanks to Friederike Bostelmann and Ugur Mertyurek for their review of this paper. Additional thanks to the University of Illinois Department of Nuclear, Plasma, and Radiological Engineering and the members of the Advanced Reactors and Fuel Cycles group.

REFERENCES

[1] P. Dimitriou, I. Dillmann, B. Singh, V. Piksaikin, K. Rykaczewski, J. Tain, A. Algora, K. Banerjee, I. Borzov, D. Cano-Ott, S. Chiba, M. Fallot, D. Foligno, R. Grzywacz, X. Huang, T. Marketin, F. Minato, G. Mukherjee, B. Rasco, A. Sonzogni, M. Verpelli, A. Egorov, M. Estienne, L. Giot, D. Gremyachkin, M. Madurga, E. McCutchan, E. Mendoza, K. Mitrofanov, M. Narbonne, P. Romojaro, A. Sanchez-Caballero, and N. Scielzo, "Development of a Reference Database for Beta-Delayed Neutron Emission," Nuclear Data Sheets, **173**, 144 (2021); https://doi.org/10.1016/j.nds.2021.04.006., URL https://www.sciencedirect.com/science/article/pii/S0090375221000168, special Issue on Nuclear Reaction Data.

[2] D. Brown, M. Chadwick, R. Capote, A. Kahler, A. Trkov, M. Herman, A. Sonzogni, Y. Danon, A. Carlson, M. Dunn, D. Smith, G. Hale, G. Arbanas, R. Arcilla, C. Bates, B. Beck, B. Becker, F. Brown, R. Casperson, J. Conlin, D. Cullen, M.-A. Descalle, R. Firestone, T. Gaines, K. Guber, A. Hawari, J. Holmes, T. Johnson, T. Kawano, B. Kiedrowski, A. Koning, S. Kopecky, L. Leal, J. Lestone, C. Lubitz, J. Márquez Damián, C. Mattoon, E. McCutchan, S. Mughabghab, P. Navratil, D. Neudecker, G. Nobre, G. Noguere, M. Paris, M. Pigni, A. Plompen, B. Pritychenko, V. Pronyaev, D. Roubtsov, D. Rochman, P. Romano, P. Schillebeeckx, S. Simakov, M. Sin, I. Sirakov, B. Sleaford, V. Sobes, E. Soukhovitskii, I. Stetcu, P. Talou, I. Thompson, S. van der Marck, L. Welser-Sherrill, D. Wiarda, M. White, J. Wormald, R. Wright, M. Zerkle, G. Žerovnik, and Y. Zhu, "ENDF/B-VIII.0: The 8th Major Release of the Nuclear Reaction Data Library with CIELO-project Cross Sections, New Standards and Thermal Scattering Data," Nuclear Data Sheets, **148**, 1 (2018); https://doi.org/10.1016/j.nds.2018.02.001., URL https://www.sciencedirect.com/science/article/pii/S0090375218300206, special Issue on Nuclear Reaction Data.

[3] T. Parish, W. Charlton, N. Shinohara, M. Andoh, M. Brady, and S. Raman, "Status of six-group delayed neutron data and relationships between delayed neutron parameters from

the macroscopic and microscopic approaches," Nuclear science and engineering, **131**, 2, 208 (1999).

[4] M. Chadwick, P. Obložinský, M. Herman, N. Greene, R. McKnight, D. Smith, P. Young, R. MacFarlane, G. Hale, S. Frankle, A. Kahler, T. Kawano, R. Little, D. Madland, P. Moller, R. Mosteller, P. Page, P. Talou, H. Trellue, M. White, W. Wilson, R. Arcilla, C. Dunford, S. Mughabghab, B. Pritychenko, D. Rochman, A. Sonzogni, C. Lubitz, T. Trumbull, J. Weinman, D. Brown, D. Cullen, D. Heinrichs, D. McNabb, H. Derrien, M. Dunn, N. Larson, L. Leal, A. Carlson, R. Block, J. Briggs, E. Cheng, H. Huria, M. Zerkle, K. Kozier, A. Courcelle, V. Pronyaev, and S. van der Marck, "ENDF/B-VII.0: Next Generation Evaluated Nuclear Data Library for Nuclear Science and Technology," Nuclear Data Sheets, **107**, 12, 2931 (2006); https://doi.org/10.1016/j.nds.2006.11.001., URL https://www.sciencedirect.com/science/article/pii/S0090375206000871, evaluated Nuclear Data File ENDF/B-VII.0.

[5] M. C. Brady, "Evaluation and application of delayed neutron precursor data," PhD Thesis (1988)URL https://www.proquest.com/dissertations-theses/evaluation-application-delayed-neutron-precursor/docview/303658613/se-2?accountid=26379, copyright - Database copyright ProQuest LLC; ProQuest does not claim copyright in the individual underlying works; Last updated - 2022-02-26.

[6] G. Keepin, T. Wimett, and R. Zeigler, "Delayed neutrons from fissionable isotopes of uranium, plutonium and thorium," Journal of Nuclear Energy (1954), **6**, 1, IN2 (1957); https://doi.org/10.1016/0891-3919(57)90178-X., URL https://www.sciencedirect.com/science/article/pii/089139195790178X.

[7] D. J. Hughes, J. Dabbs, A. Cahn, and D. Hall, "Delayed Neutrons from Fission of U^{235}," Phys. Rev., **73**, 111 (1948); 10.1103/PhysRev.73.111., URL https://link.aps.org/doi/10.1103/PhysRev.73.111.

[8] D. J. Loaiza, G. Brunson, R. Sanchez, and K. Butterfield, "Measurements of Absolute Delayed Neutron Yield and Group Constants in the Fast Fission of 235U and 237Np," Nuclear

Science and Engineering, **128**, 3, 270 (1998); 10.13182/NSE98-A1955., URL https://doi.org/10.13182/NSE98-A1955.

[9] D. J. Loaiza and F. E. Haskin, "Dominant Delayed Neutron Precursors to Model Reactivity Predictions for Multiple Fissioning Nuclides," Nuclear Science and Engineering, **134**, 1, 22 (2000); 10.13182/NSE00-A2097., URL https://doi.org/10.13182/NSE00-A2097.

[10] W. Wieselquist and R. A. Lefebvre, "SCALE 6.3.1 User Manual," ORNL/TM-SCALE-6.3.1, Oak Ridge National Laboratory (ORNL), Oak Ridge, TN (United States) (2023); 10.2172/1959594., URL https://www.osti.gov/biblio/1959594.

[11] R. E. Peterson and G. A. Newby, "AN UNREFLECTED U-235 CRITICAL ASSEMBLY," Nuclear Science and Engineering, **1**, 112 (1956)URL https://api.semanticscholar.org/CorpusID:123304404.

[12] W. B. Wilson, R. T. Perry, W. Charlton, T. Parish, and E. Shores, "SOURCES: a code for calculating (α, n), spontaneous fission, and delayed neutron sources and spectra," Radiation protection dosimetry, **115**, 1-4, 117 (2005).

[13] J. K. Tuli et al., "Evaluated nuclear structure data file," A Manual for Preparation of Data Sets-National Nuclear Data Center Brookhaven National Laboratory PO Box, **5000**, 11973 (2001).

[14] D. Saphier, D. Ilberg, S. Shalev, and S. Yiftah, "Evaluated Delayed Neutron Spectra and Their Importance in Reactor Calculations," Nuclear Science and Engineering, **62**, 4, 660 (1977); 10.13182/NSE77-A15209., URL https://doi.org/10.13182/NSE77-A15209.

[15] M. C. Brady and T. R. England, "Delayed Neutron Data and Group Parameters for 43 Fissioning Systems," Nuclear Science and Engineering, **103**, 2, 129 (1989); 10.13182/NSE103-129., URL https://doi.org/10.13182/NSE103-129.

[16] G. Rudstam, "Six-Group Representation of the Energy Spectra of Delayed Neutrons from Fission," Nuclear Science and Engineering, **80**, 2, 238 (1982); 10.13182/NSE82-A21428., URL https://doi.org/10.13182/NSE82-A21428.

[17] T. R. England, W. B. Wilson, R. E. Schenter, and F. M. Mann, "Aggregate Delayed Neutron Intensities and Spectra Using Augmented ENDF/B-V Precursor Data," Nuclear Science and Engineering, **85**, 2, 139 (1983); 10.13182/NSE83-A27422., URL https://doi.org/10.13182/NSE83-A27422.

[18] C. Tofallis, "Least squares percentage regression," Journal of Modern Applied Statistical Methods (2009).

[19] C. L. Lawson and R. J. Hanson, Solving least squares problems, SIAM (1995).

[20] M. I. Radaideh, W. A. Wieselquist, and T. Kozlowski, "A new framework for sampling-based uncertainty quantification of the six-group reactor kinetic parameters," Annals of Nuclear Energy, **127**, 1 (2019).

[21] R. Tuttle, "Delayed-neutron yields in nuclear fission," Proc. Second Consultants Meeting on Delayed Neutron Properties, vol. 29 (1979).

[22] R. Kinsey, L. Stewart, R. LaBauve, P. Young, A. Horsley, G. Hale, M. Battat, H. Perkins, C. Cowan, C. Fu, F. Perey, D. Foster, B. Magurno, D. Larson, M. Allen, M. Drake, C. Philis, A. Smith, R. Howerton, F. Mann, A. Prince, T. Burrows, S. Mughabghab, M. Divadeenam, R. Howerton, M. Bhat, H. Takahashi, B. Leonard, K. Stewart, D. Sargis, T. Maung, J. Otter, C. Dunford, E. Ottewitte, W. Henderson, J. Zwick, E. Kujawski, L. Weston, and R. Wright, "ENDF/B Summary Documentation," , Brookhaven National Laboratory (1979).

[23] W. Wilson, T. England, R. Schenter, and F. Mann, "Delayed neutron study using ENDF/B-VI basic nuclear data," Progress in Nuclear Energy, **41**, 1, 71 (2002); https://doi.org/10.1016/S0149-1970(02)00006-9., URL https://www.sciencedirect.com/science/article/pii/S0149197002000069.

[24] T. England and B. Rider, "Status of fission yield evaluations," , Los Alamos National Laboratory (LANL), Los Alamos, NM (United States) (1983).